SAND2015-7148R

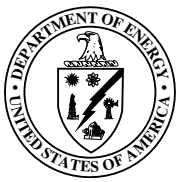

Sandia National Laboratories

Operated for the U.S. Department of Energy by

Sandia Corporation

Albuquerque, New Mexico 87185

date: August 5, 2015

to: Distribution

from: Justin Crum, Org. 01554, MS-0840

subject: Finite Element Simulations to Explore Assumptions in Kolsky Bar Experiments

The chief purpose of this project has been to develop a set of finite element models that attempt to explore some of the assumptions in the experimental set-up and data reduction of the Kolsky bar experiment. In brief, the Kolsky bar, sometimes referred to as the split Hopkinson pressure bar, is an experimental apparatus used to study the mechanical properties of materials at high strain rates. Kolsky bars can be constructed to conduct experiments in tension or compression, both of which are studied in this paper. The basic operation of the tension Kolsky bar (Fig. 1(a)) is as follows: compressed air is inserted into the barrel that contains the striker; the striker accelerates towards the left and strikes the left end of the barrel producing a tensile stress wave that propogates first through the barrel and then down the incident bar, into the specimen (Fig. 1(b)), and finally the transmission bar. In the compression case, the striker instead travels to the right and impacts the incident bar directly. As the stress wave travels through an interface (e.g., the incident bar to specimen connection), a portion of the pulse is transmitted and the rest reflected. The incident pulse, as well as the transmitted and reflected pulses are picked up by two strain gauges installed on the incident and transmitted bars as shown. By interpreting the data acquired by these strain gauges, the stress/strain behavior of the specimen can be determined.

In order to analyze and evaluate the experimental data reduction procedure used to obtain the mechanical properties of test specimens, a circular method is proposed and used here. Analysis of the specimen behavior requires stress/strain data as input. After predefining the behavior of the specimen, a finite element model of the Kolsky bar and specimen can

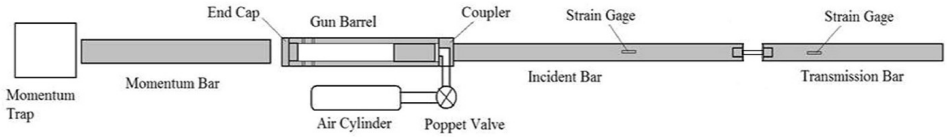

(a) Kolsky bar (Tension configuration shown) (Song et al, 2013)

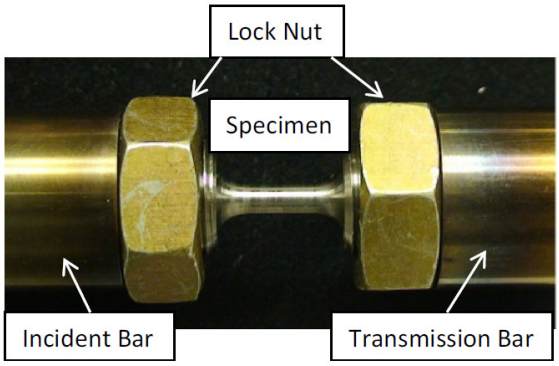

(b) Tension Specimen (Song et al, 2015)

Figure 1. Experimental schematic of the tension Kolsky bar.

be used to simulate the experiment. The simulation results can, in turn, be used to give a stress/strain curve according to the procedure used in the lab (Song et al, 2015). This data can then be compared with the input information to evaluate how effectively the data reduction procedure interprets the material behavior.

Before this method was utilized, several trade studies were performed to better understand stress wave generation, shaping, propagation, and detection. A model of a propagating compressive stress wave was used for analysis. This stress wave (referred to as "the pulse") that propagates through the incident bar is approximately twice the length of the striker and its magnitude is proportional to the impact velocity. Additionally, this pulse can be further altered by the presence of a pulse shaper. A pulse shaper is a small metal disk placed at the point where the striker impacts either the gun barrel end cap (for tension) or the incident bar (for compression). Its primary function is to reduce the high frequency content of the pulse to reduce the dispersion effects present in the stress wave and also to create a sufficiently long rise time in the pulse to allow for equilibration of the specimen. In all of these trade studies, the model was simplified to include just a striker and an incident bar, both of the same material. Identical to the incident bar in the full model, this bar (MAR300 RD AMS6514 steel; $E = 27.5$ GPa, $\rho = 0.289\text{lb/in}^3$, $\nu = 0.3$) was 144 inches in length and 1 inch in diameter. The axial stress on the incident bar surface was output at a location 96 inches from the impacted end. A few standards were adopted for the other components in the simulation. A standard 1 inch diameter striker, 12 inches in length, was used to strike the pulse shaper at a velocity of 139.4 in/s. This velocity was chosen to cause a nominal stress wave, 10 ksi in magnitude, to propagate through the bar. As for the pulse shaper, a trade study (explained below) was used to select a 27 gauge piece of annealed c11000 copper 11/32 inches in diameter as the default shaper. When not the focus of a study, these above

mentioned specifications were held constant. In all calculations presented, the finite element model was axisymetric and used four node elements with reduced integration and hourgalss control (Element type CAX4R in Abaqus/Explicit).

A study exploring the effects of the striker's size and shape on pulse generation was performed. The strikers tested were of lengths 6, 7.5, 12, and 24 inches along with a 12 inch tapered striker. The 7.5 inch striker was chosen because of its equivalent volume, and therefore mass, to the tapered striker. Two studies were performed: one without a pulse shaper and one with a 27 gauge, 11/32 inch diameter copper piece. The material properties used for the copper were pulled from experimental data provided by Sandia's shock laboratory. This shaper was chosen because it creates an approximately 10 ksi magnitude stress wave that has a nominal rise time equal to the pulse length at low velocities. The velocity of striker impact was held constant in both studies. In the study with no pulse shaper (Fig. 2(a)), all strikers (with the exception of the tapered striker) yielded an identical stress pulse shape, with the only variance being the length of the pulse. The duration of each of the pulses was directly proportional to the length of the striker bars used. For the case of the tapered striker, the shape of the stress wave resembled the shape of the striker itself. Geometrically, the tapered portion of the striker corresponds to two-thirds of its total length, and impact occurs at the end with constant cross-section and largest diameter. The pulse, likewise, shows that the trailing two-thirds of the pulse are tapered. In fact, a geometric correlation is present in every resulting pulse, whether generated by a cylindrical or tapered striker. Similarly, the data from the study with the pulse shaper (Fig. 2(b)) shows that all strikers tested have overlapping rising curves, but diverge at a time proportional to the relative lengths of the strikers themselves. As for the tapered striker, its pulse again begins to taper at a time representative of its geometry. The baseline curve in this figure, and in subsequent figures, is the pulse generated by a 12 inch striker with no pulse shaper and is shown for comparison purposes.

In another study, the impact velocity of the striker was changed while its length was held constant at 12 inches and the pulse shaper remained a 27 gauge, 11/32 inch diameter copper piece. The initial gap between the striker and the pulse shaper in the model was calibrated so that impact occurred at the same frame in all simulations (i.e., the distance was doubled when the velocity was doubled). The conclusion of the velocity analysis (Fig. 3) was that the magnitudes of the stress waves were directly proportional to the initial velocity of the striker. When the magnitude of the stress wave approached 40 ksi, the copper pulse shaper deformed in a way unlike the other simulations and therefore the pulse had a different shape. This is representative of a case where the shaper reaches maximum deformation and the pulse takes on a more "square" shape. No amount of mesh refinement seemed to affect these results.

An extensive study was performed to analyze how variances in thickness and diameter of the pulse shaper affected the actual shape of the stress wave. Three diameters (5/32, 11/32, and 17/32 inch) were studied in conjunction with four thickness (10, 16, 21, and 27 gauge) totaling twelve simulations. A baseline simulation that contained no pulse shaper was used for comparison purposes. Two overarching conclusions can be drawn from the results of the study. With respect to changes in the diameter (Fig. 4), as the diameter decreased, keeping

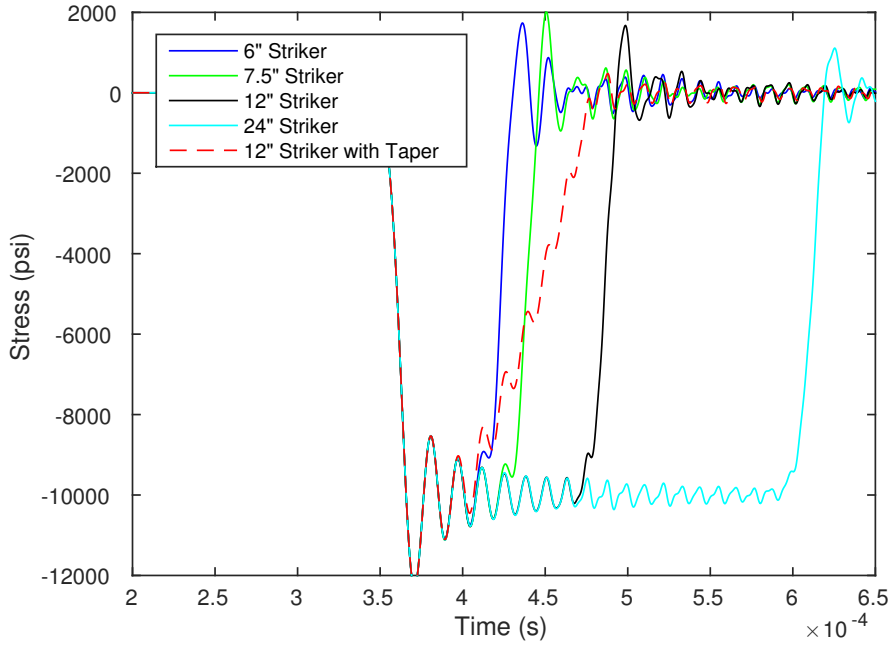

(a) No pulse shaper

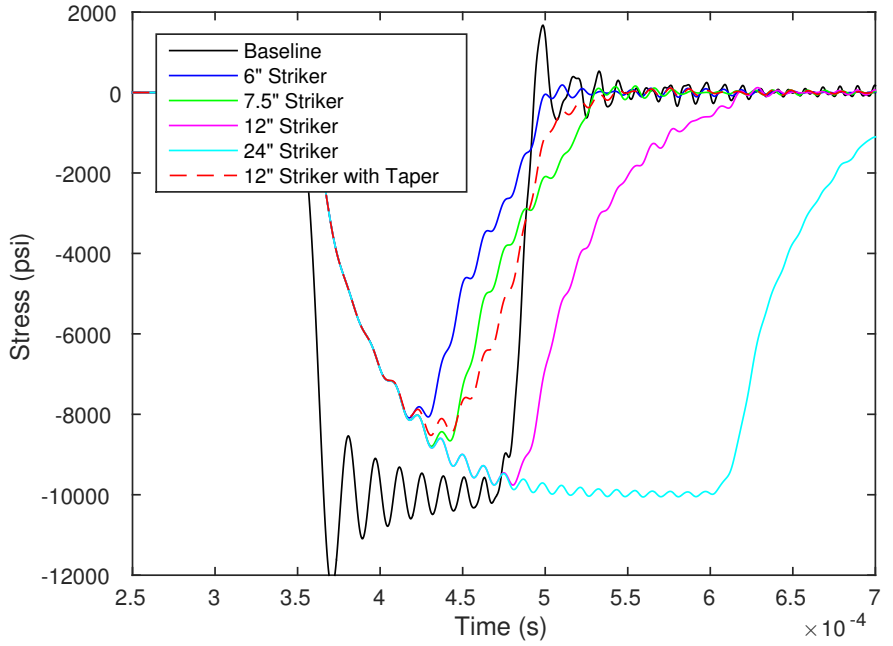

(b) 27 gauge, 11/32 inch diameter copper pulse shaper

Figure 2. Effects of striker lenght and shape on pulse creation. Striker velocity = 139.4 in/s.

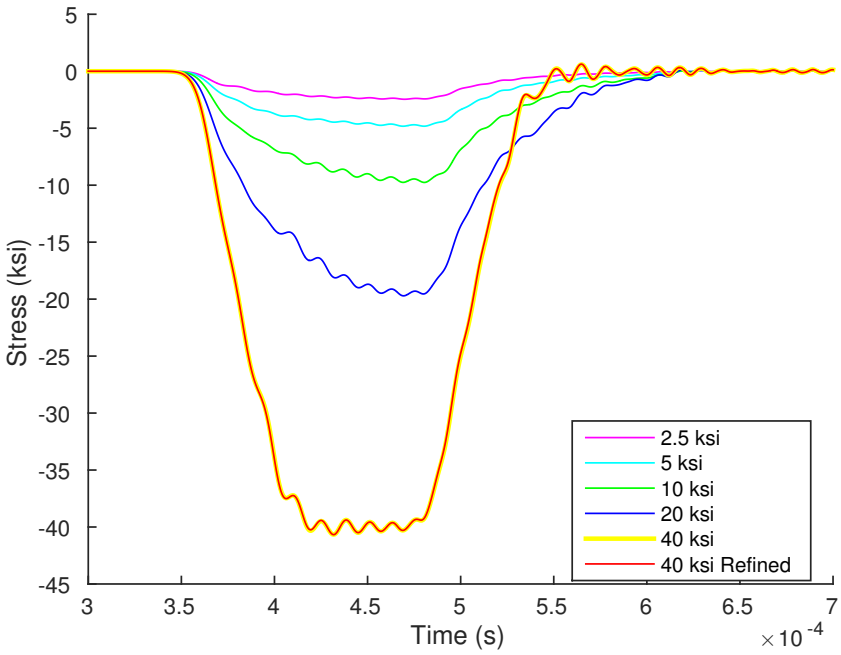

Figure 3. Effects of striker velocity (in terms of the stress pulse amplitude) on pulse creation when a pulse shaper is present. Striker length = 12 inches. 27 gauge, 11/32 inch diameter copper pulse shaper.

thickness constant, the magnitude of the stress pulse decreased and the length increased. Additionally, the presence of high-frequency oscillations due to dispersion were significantly reduced as the diameter of the pulse shaper decreased. Perhaps more intuitively, when the thickness was varied (Fig. 5), these shaping effects were increased as the thickness also increased. If the extreme combinations of these two variables are studied (Fig. 6), the observed differences between the baseline and resulting pulses are drastic. The thickest pulse shaper with the smallest diameter caused the magnitude of the stress wave to decrease by a factor of three and the length to increase fourfold when compared to the baseline pulse. Conversely, the thinnest example with the largest diameter barely caused any change in the magnitude or length of the stress pulse relative to the baseline; the rise and decline times are only slightly lengthened. It should be noted at this point that the pulses at the velocity displayed in the figures would not be ideally shaped for the experimental purposes of the Kolsky bar. An optimal pulse shaper for a given set of experimental conditions would, in actuality, do little more than tune the nominal square pulse's rise time. Thus, shapers that altered the nominal pulse more would be only be appropriate in higher energy impacts. Simulations with a sufficiently low impact velocity were used only to magnify the different shaping effects.

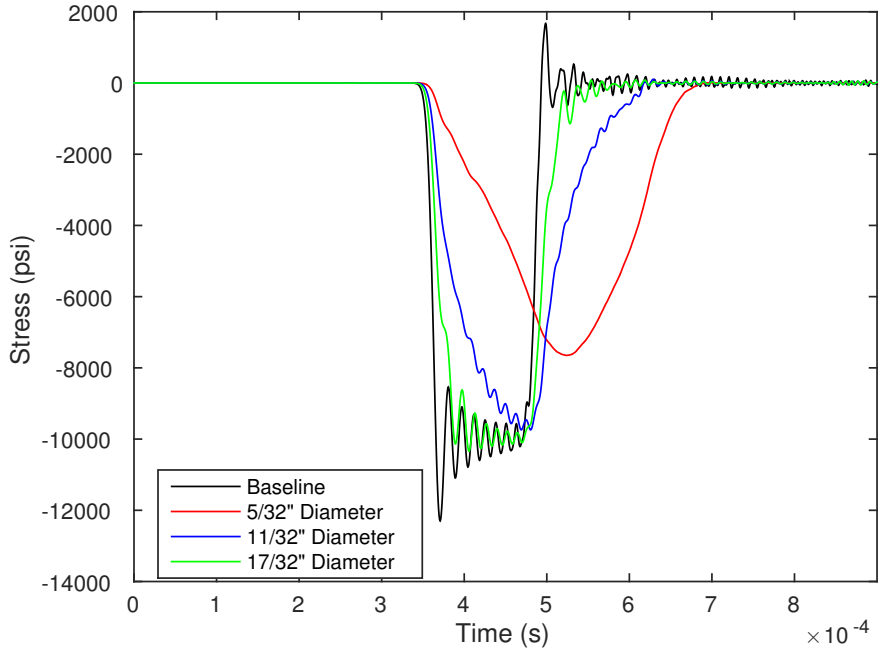

Figure 4. Effects of shaper diameter on the resulting pulse. Striker length = 12 inches. Striker velocity = 139.4 in/s.

Finally, to test the variance in readings across the radius of the bar, a few simulations were run where data were extracted from elements at different radii. The differences evident between the stresses at the center of the bar and the outer edge are less than 1.5 percent of the main pulse's magnitude. Furthermore, these differences are only evident when dispersion

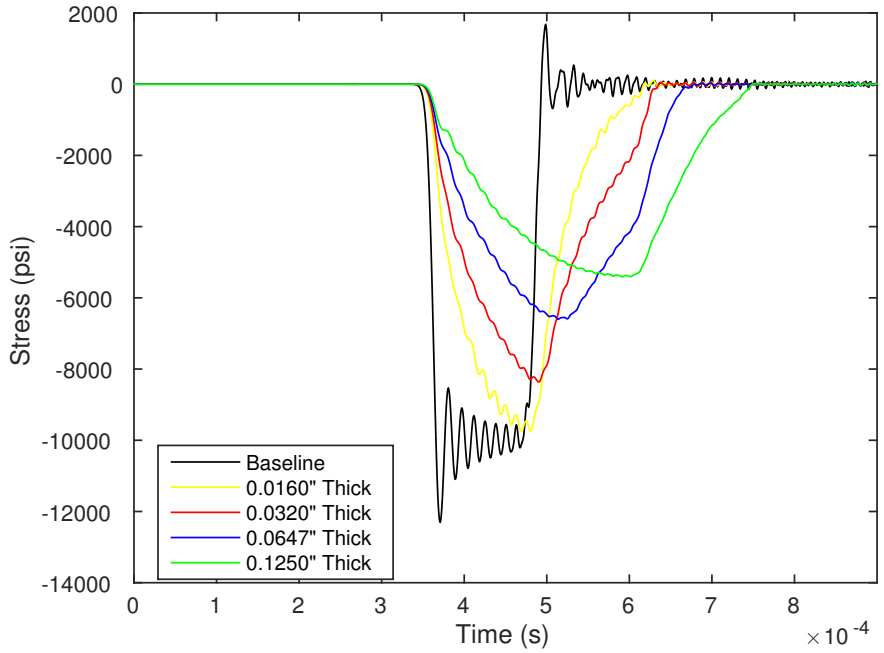

Figure 5. Effects of shaper thickness on the resulting pulse. Striker length = 12 inches. Striker velocity = 139.4 in/s.

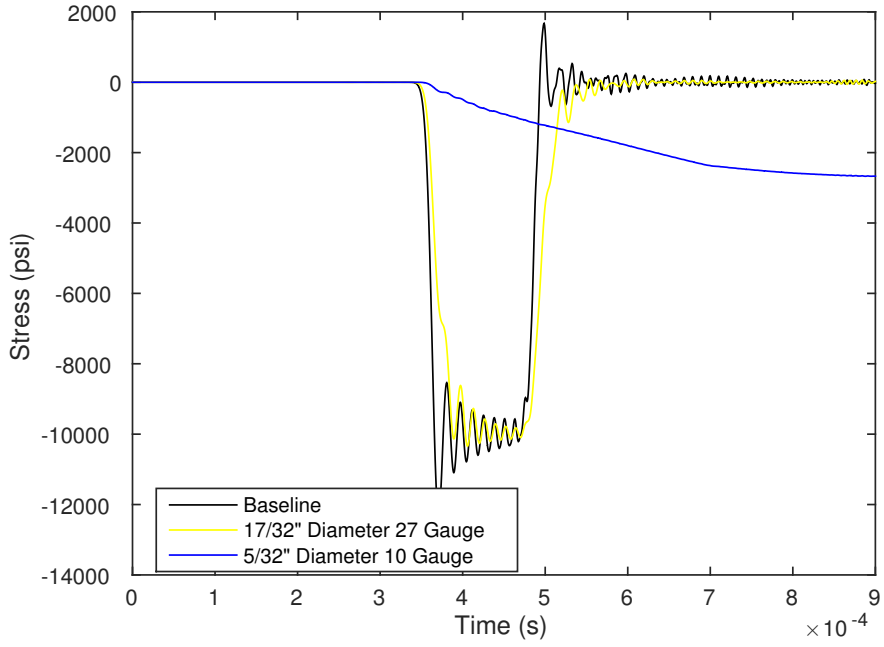

Figure 6. Cases of extreme shaping effects. Striker length = 12 inches. Striker velocity = 139.4 in/s.

effects are present. The two extreme pulse shapers from the thickness and diameter study were used. For the thick shaper, high-frequency oscillations were barely observable on the scale of the main pulse and thus variances between the readings at the center of the bar and the outer radius were indistinguishable. The thin shaper, on the other hand, did display noticeable dispersion effects and the readings differed at the troughs and peaks of these oscillations. The broad shape of the main pulse, however, was not affected by the location of the readings. With these effects being insignificant, all other analyses were performed using the element at the outer radius to approximate the physical locations of strain gauges in lab tests.

After these trade studies had been performed, the first attempts to model Kolsky bar tests were pursued. The data reduction procedure from tension Kolsky bar tests necessitate a few assumptions that can be explored using this model. In a tension Kolsky bar experiment, the purity of the reflected pulse, for example, is diminished by the complex threaded interfaces between the specimen and the bars. As numerous reflected pulses begin to overlap, the readings in the incident bar's strain gauge become muddled. Because the reflected pulse can be unreliable, this creates the need for additional data acquisition methods to more accurately determine the strain in the specimen. Currently, lasers are used to track the displacements at the ends of the bars (Fig. 7). A lens disperses the laser into a line that spans the ends of both the incident and transmission bars. The amount of light that is not obstructed by the bars is redirected by a prism mirror, through another lens, and into a detector. This method can accurately detect the displacements of the ends of the bars; however, this measurement is not local to the gauge section in the specimen. A few assumptions are thus needed to estimate the stretch over this portion.

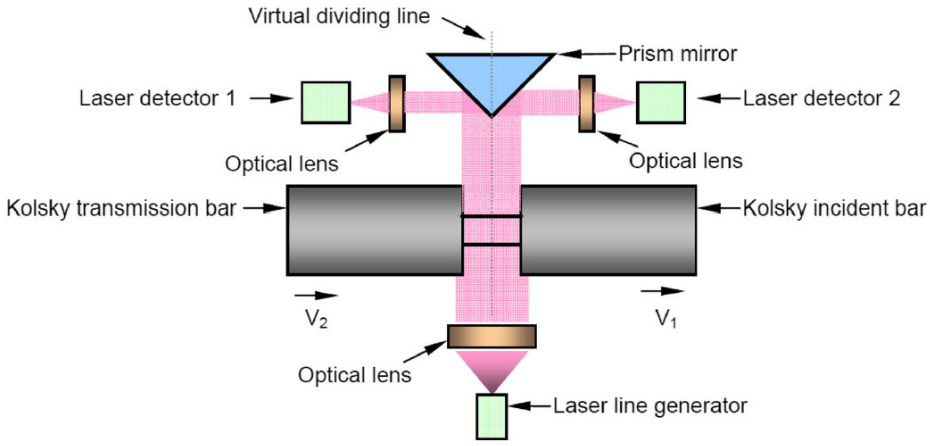

Figure 7. Laser setup used to track the displacements of the bar ends (from Song et al, 2013).

The stress in the specimen can be calculated based on wave propagation principles using the equation

$$\sigma_s = \frac{A_b}{A_s} E_b \epsilon_t, \tag{1}$$

where A_b and A_s are the cross-sectional areas of the transmission bar and specimen gauge section respectively, E_b is the modulus of the transmission bar, and ϵ_t is the strain read by the transmitted strain gauge. The specimen strain calculation is not quite as simple. From Fig. 8(a), the specimen strain is given by the equation

$$\epsilon_s = \frac{\Delta l_s}{l_s} = \frac{\Delta L_t - \Delta l_e}{l_s}, \tag{2}$$

where

$$\Delta L_t = u_t - u_i \tag{3}$$

and u_t and u_i are the displacements of the transmitted and incident bar/specimen interfaces measured by the laser. The stretch of the specimen "shoulders," Δl_e, can be estimated by assuming linearly elastic material behavior and uniaxial stress. A simple strength of materials analysis gives

$$\Delta l_e = \frac{2 A_b E_b \epsilon_t}{E_s} \int_0^{l_e} \frac{dx}{\pi (R + r_0 - \sqrt{R^2 - x^2})^2}. \tag{4}$$

where R is the radius of curvature in the shoulder and r_0 is the radius of the specimen gauge section's cross-section as shown in Fig. 8(b).

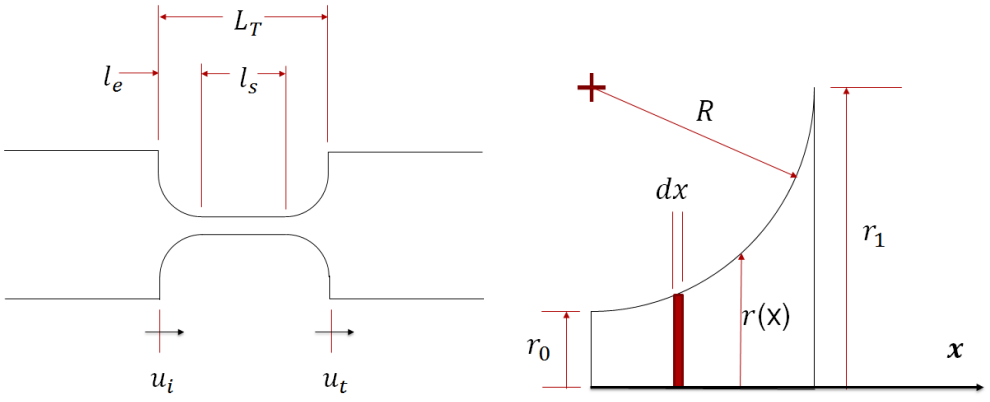

(a) Specimen **(b)** Specimen Shoulder

Figure 8. Schematic for specimen strain calculations

The strain ϵ_s represents an assumed average strain over the specimen gauge section. A stress/strain plot can then be calculated from equations (1) and (2) by using only the transmitted strain gauge output and the laser measurements, thus eliminating the need for a clean reflected pulse.

Because not all measurements are made locally at the specimen, time history corrections have to be made for the strain gauge data. The speed of the stress pulse as it propagates through the bar is known so the time lag between the measurements of ϵ_s and σ_s can be easily determined since the location of the strain gauge in the transmitted bar is known. In the shock lab's standard calculations, an additional amount of time is added while the specimen reaches force equilibrium. This is assumed to be approximately the length of time in three round trips through the specimen at the wave speed. When analyzing the results of the simulations discussed below, this additional small time correction factor was unnecessary and was not used.

The finite element model is composed of an axisymmetric mesh in Abaqus/Explicit. It is capable of simulating the dynamics of the experiment and its strength is its ability to determine more quantities than are possible in the lab (Fig. 9). In addition to tracking the displacements at the ends of the bars, it is possible to directly track the displacements at the edges of the gauge section. In these simulations, the above mentioned quantities are tracked along with the relative displacements at the edges of the middle fifty percent of the gauge section. These extra displacements allow for evaluation of the data reduction process.

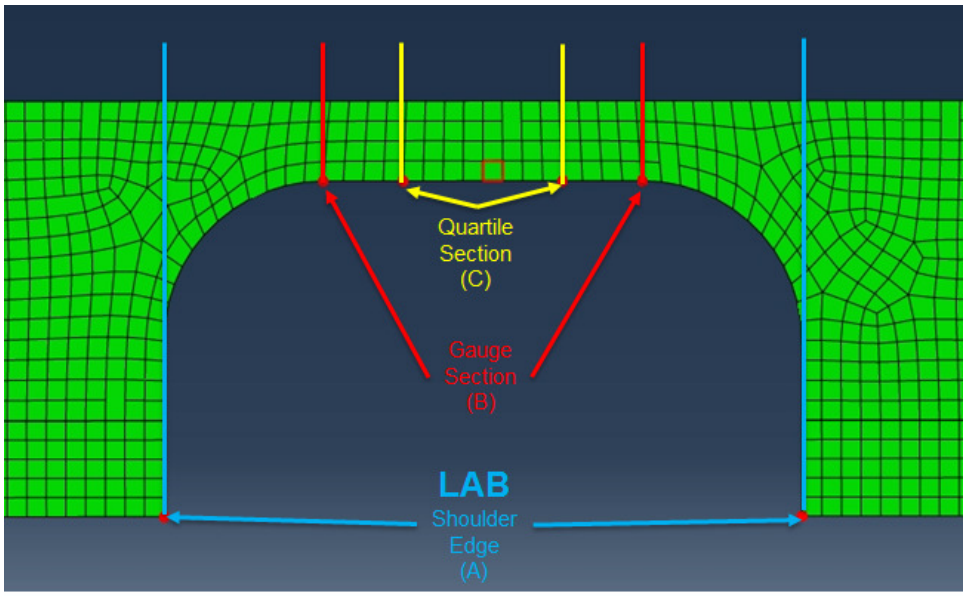

Figure 9. Location of tracked nodes in the Finite Element Model. Pictured is an axisymmetric mesh representing half of the specimen cross-sectional area.

When an elastic-perfectly plastic true stress/strain curve is applied to the specimen in the simulation, the plastic strain (Fig. 10(a)) localizes at the center of the test section immediately after yield. In the simulation, an arbitrary value of 0.08 for the plastic strain was selected as the failure criterion for model. The final configuration of the specimen exhibits a break at the center. An analysis of the output stress/strain data reveals a source of potential error in the experimental data reduction process. Stress/strain calculations based on the measurements made at the end of the bars and also over just the gauge section significantly underpredict the strain values (Fig. 10(b), curves A and B) compared to the measurements

made over the center half of the specimen (curve C). This can be explained by the localization of the plastic strain near the center (Fig. 10(a)) since the calculations assume average deformation across the specimen. The strain is calculated over the full length of the gauge section and therefore is measured less than the actual strain magnitudes at the center. While this issue demonstrates the error in one assumption, it does support the assumption that the shoulders behave elastically. In this simulation with no plastic hardening, no plastic strain propagated into the shoulder. Finally, note that the engineering stress-strain curve has decreasing stress starting right after yield, as expected from the assigned elastic-perfectly plastic true stress-strain curve.

Another simulation was run that embodied a bilinear hardening scheme. The linear hardening curve was set to have a true stress/strain slope two percent of the elastic modulus. Because of the hardening characteristics of this material definition, a significant amount of plastic strain propagated into the shoulders of the specimen (Fig. 11(a)). In this simulation, the same arbitrary failure criterion as the previous simulation was used. The plastic hardening in the specimen shoulders is immediately evident in the output stress/strain curve; the data measured at the edges of the bars greatly overpredict the strain values in the specimen because the plastic strain present in the shoulder is not subtracted from the total change in length, ΔL_t (Fig. 11(b), curve A). Only the elastic deformation is accounted for. This demonstrates that, for materials with significant hardening, assuming that the shoulders of the specimen only deform elastically does not accurately represent their actual behavior. However, when the strain is calculated using the nodes at the edges of the gauge section (curve B), the output stress/strain data closely reflects the input curve. This can be explained by analyzing the plastic strain in the simulation; it is distributed almost uniformly over the entire gauge length. This means that for situations with materials that exhibit more hardening behavior, the strain over the gauge section of the specimen is approximately uniform, at least prior to the onset of necking, which was not achieved in the simulation.

Up until this point, all simulations had incited a specimen strain rate of approximately 175/s. All further studies were conducted at rates on the order of ten times greater. First, a simulation was ran that mimicked the perfectly plastic model, where the striker was impacted at ten times the velocity. The results appeared to have the same trends as the previous simulation, but contained more drastic stress oscillations (Fig. 12). Despite these increased dispersion effects at the higher strain rate, the same conclusions about the data reduction assumptions can be reasonably drawn.

To make a first attempt at testing the model's ultimate purpose, material data from a previous test in the lab was input into the material model. This material definition (Johnson-Cook) contained rate dependent information. After the simulation ran, the data from both experiment and simulation were plotted and the stress/strain curves compared (Fig. 13). Qualitatively, the curves are similar in their stress plateau and yield stress, but fail at significantly different strains. When the differences in the physical model (e.g., old vs. new specimen geometry, different bar sizes, pulse shaper selection) are taken into account, no strong conclusions can be drawn from the comparison. It was also identified in the simulation that the strain rate was not constant leading up to failure (Fig. 14). This suggests that, in

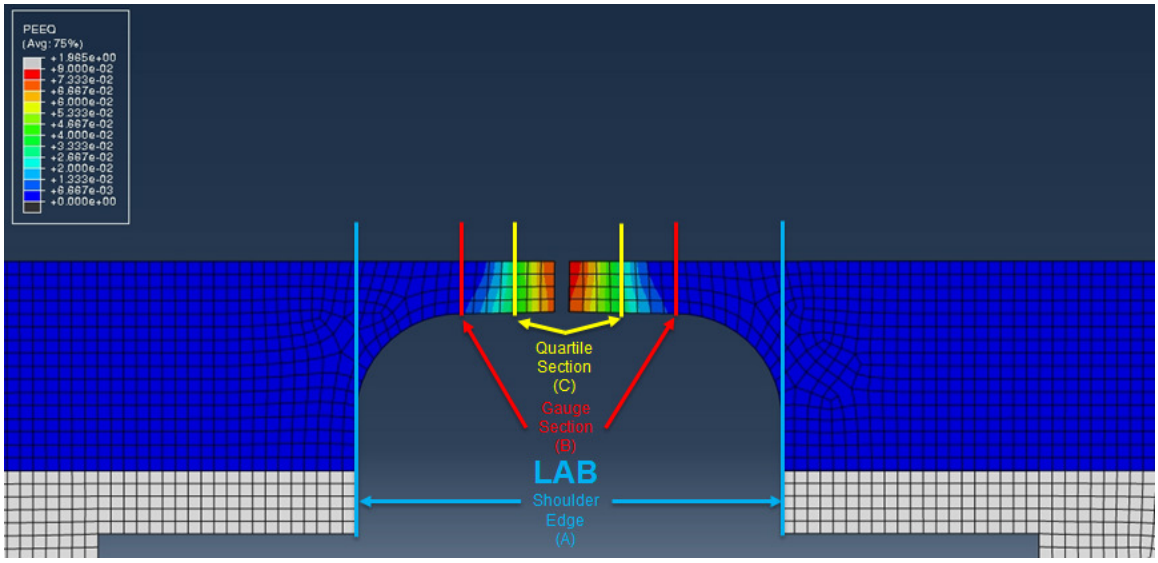

(a) Plastic Strain

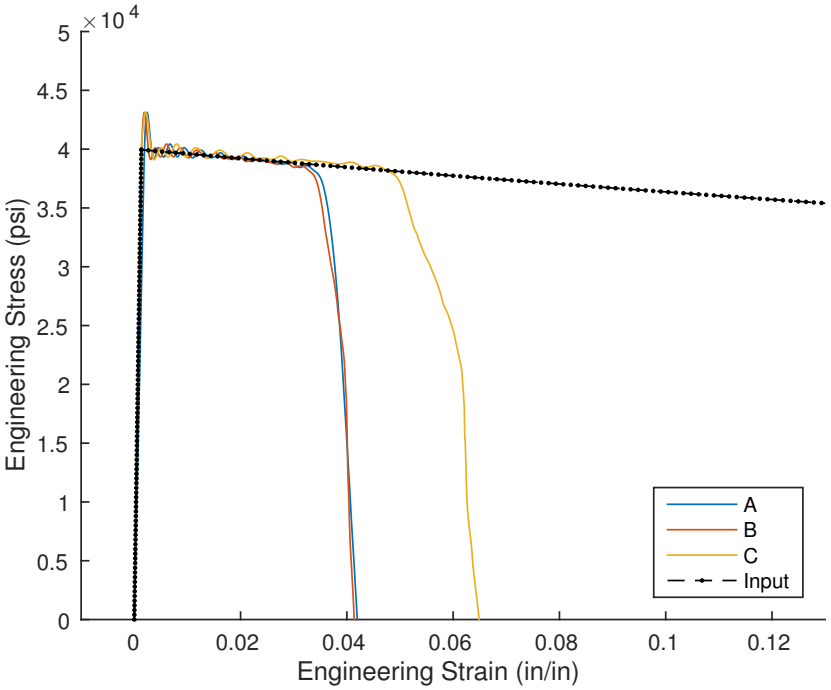

(b) Perfectly Plastic Stress/Strain Curve

Figure 10. Results assuming elastic-perfectly plastic material behavior

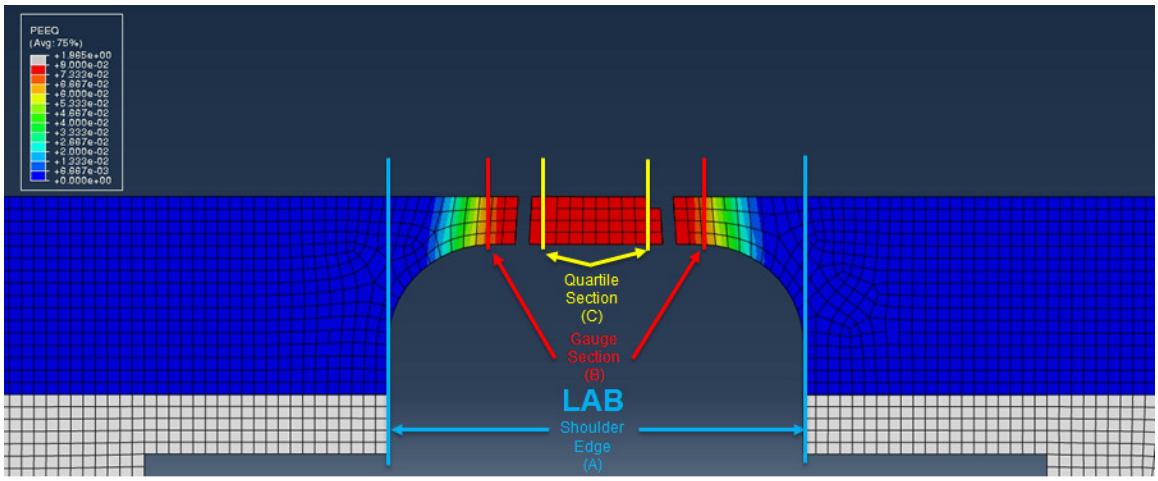

(a) Bilinear Hardening

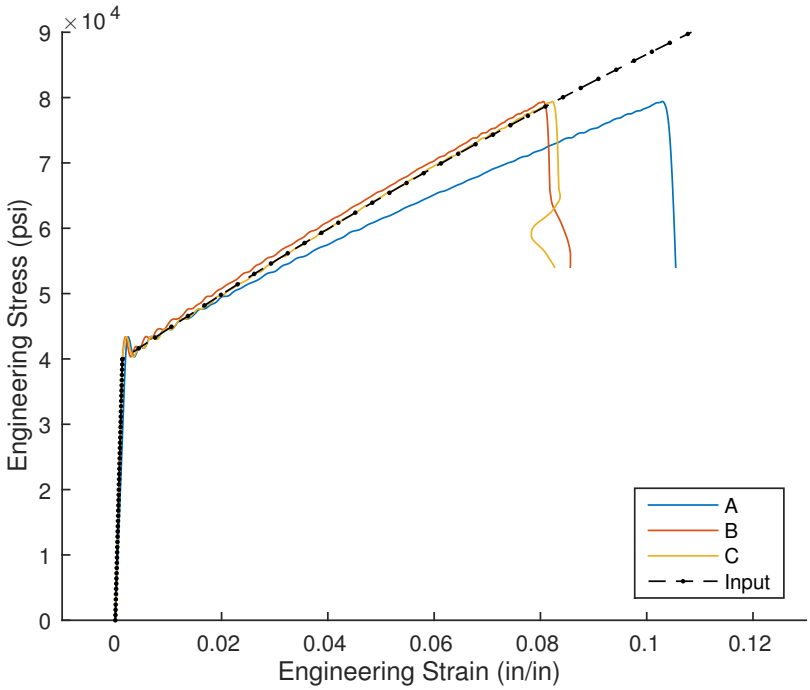

(b) Bilinear Hardening Stress/Strain Curve

Figure 11. Results assuming a bilinearly hardening material model

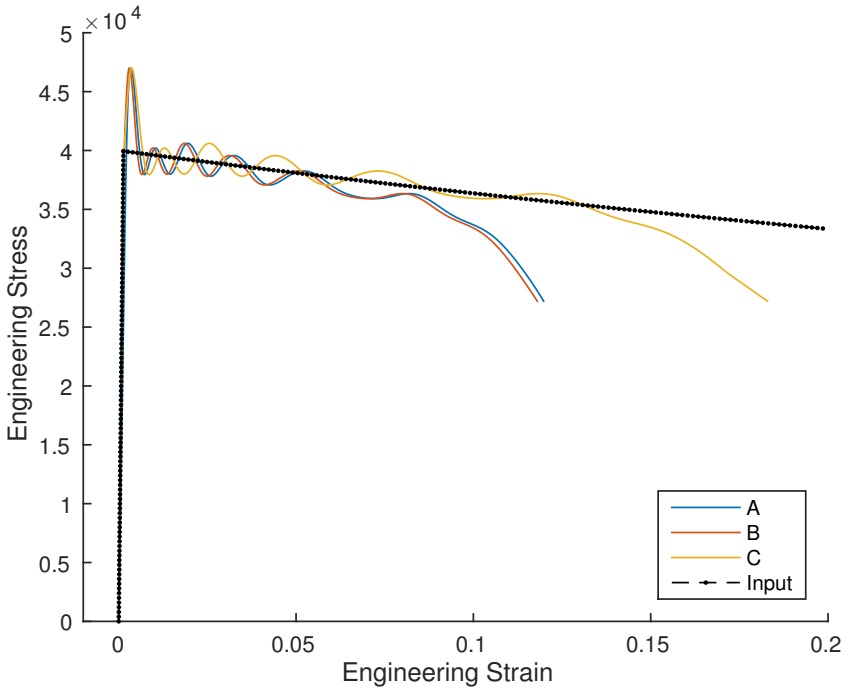

Figure 12. Basic high strain rate behavior similar to low strain rate behavior for a perfectly plastic material definition

the least, an identical pulse shaper to that used in the experiments should be inserted into the finite element model before an effective comparison can be made. However, either recreating the simulation geometry to match the old test setup or selecting a more recent experiment to study may be the only worthwhile comparison for future investigations.

One additional detail of interest became evident during the analysis of this simulation. While the stress/strain curve associated with the laser displacement tracking (A) closely followed the curve corresponding to the direct displacement measurements at the edge of the gauge section (B), the two curves actually did not reflect the same moduli values over the elastic regime (Fig. 13). When strains were calculated using the displacements at the ends of the bars, the calculated modulus was only ninety percent of the input material definition in the finite element model. However, for both the measurements over the gauge section and middle fifty percent of the gauge section, the calculated moduli were within one percent of the input value. To see if this effect was more pervasive than in just this one simulation, several other previous simulations were also scrutinized. For the high strain rate, perfectly plastic simulation, the modulus measured according to the laser method was only seventy percent of the input data. This would suggest that even when the whole model is in the elastic regime, the specimen shoulders are actually stretching more than calculated by equation (4). This was verified from the model's output data but is an area of future investigation.

In conclusion, a set of finite element models have been created to aid in the improvement of the data reduction procedure used in tension Kolsky bar experiments. These models

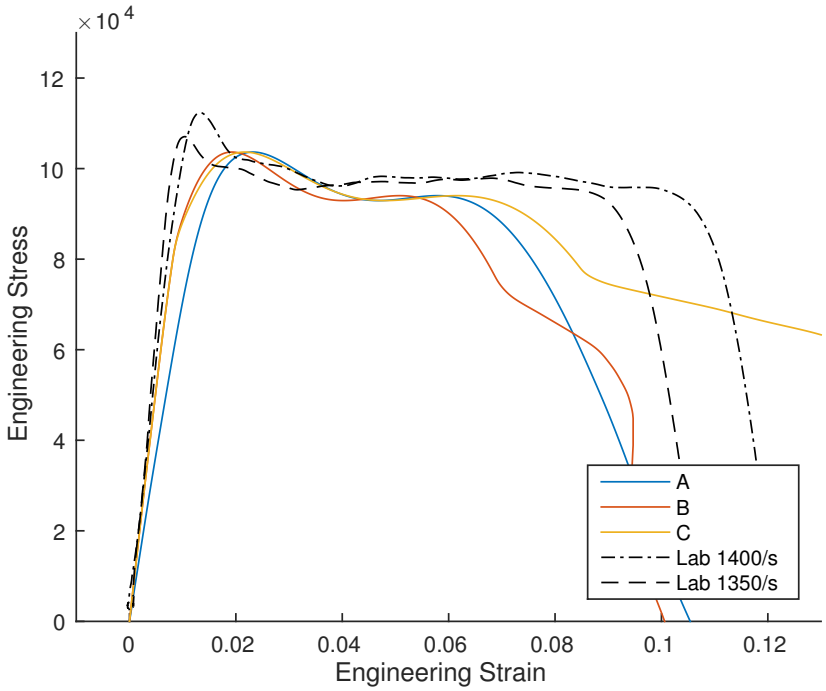

Figure 13. Experimental data and simulated data with input based on experimental results

are capable of evaluating the assumptions in the data reduction and identifying potential sources of error. In the future, modifications to the specimen design can be explored through further simulations to improve the data reduction procedure and reduce the errors in the measurement of material stress/strain response.

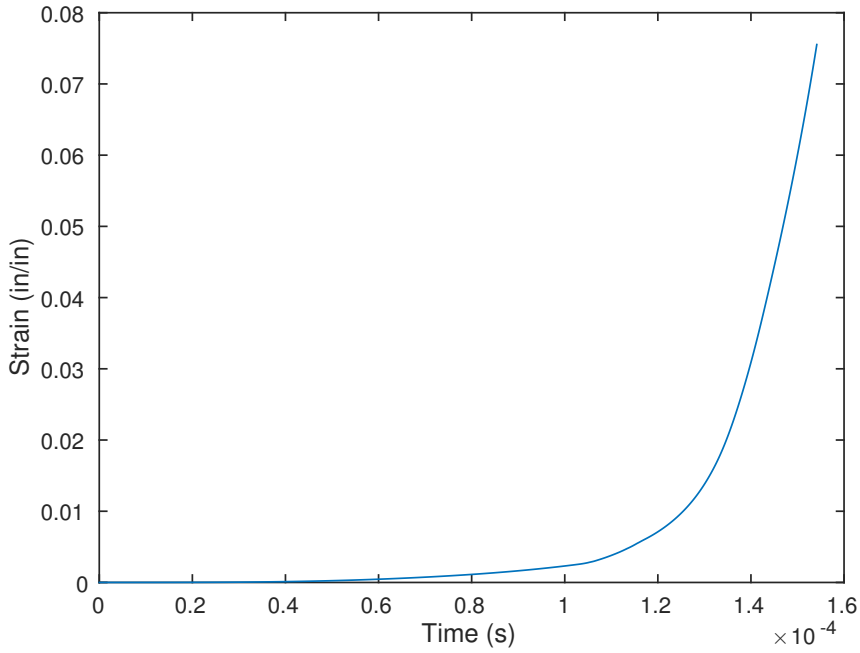

(a) Strain

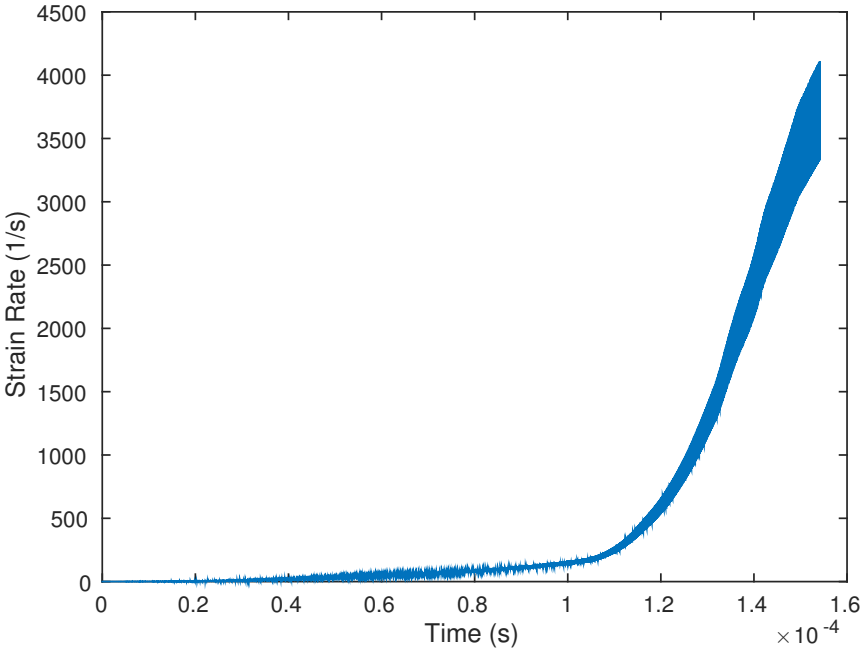

(b) Strain Rate

Figure 14. Strain response calculated in the simulations shown in Fig. 13

References

B. Song, B.R. Antoun, H. Jin; 2013. Dynamic Tensile Characterization of a 4330-V Steel with Kolsky bar Techniques; Experimental Mechanics, Volume 53, pp.1519-1529.

B. Song, P. E. Wakeland, M. Furnish; 2015. Dynamic Tensile Characterization of Vascomax Maraging C250 and C300 Alloys; J. dynamic behavior mater, Volume 1, pp.153-161.

Sandia National Laboratories is a multi-program laboratory managed and operated by Sandia Corporation, a wholly owned subsidiary of Lockheed Martin Corporation, for the U.S. Department of Energy's National Nuclear Security Administration under contract DE-AC04-94AL85000.

External Distribution:

Internal Distribution:

MS-0840	E. Corona	Org. 01554
MS-0557	B. Sanborn	Org. 01558
MS-0557	B. Song	Org. 01558
MS-0840	H. Fang	Org. 01554
MS-0840	J. Redmond	Org. 01550